Electronic Supplementary Material (ESI) for CrystEngComm.
This journal is © The Royal Society of Chemistry 2017

ELECTRONIC SUPPORTING INFORMATION

Galvanic replacement based Cu_2O self-templating strategy for the synthesis and application of Cu_2O–Ag heterostructures, and hollow metallic (Ag, Au-Ag) mesocages

Rangarajan Bakthavatsalam, and Janardan Kundu*

Physical and Materials Chemistry Division, CSIR-National Chemical Laboratory,
Dr. Homi Bhabha Road, Pashan, Pune, Maharashtra, 411008, India.

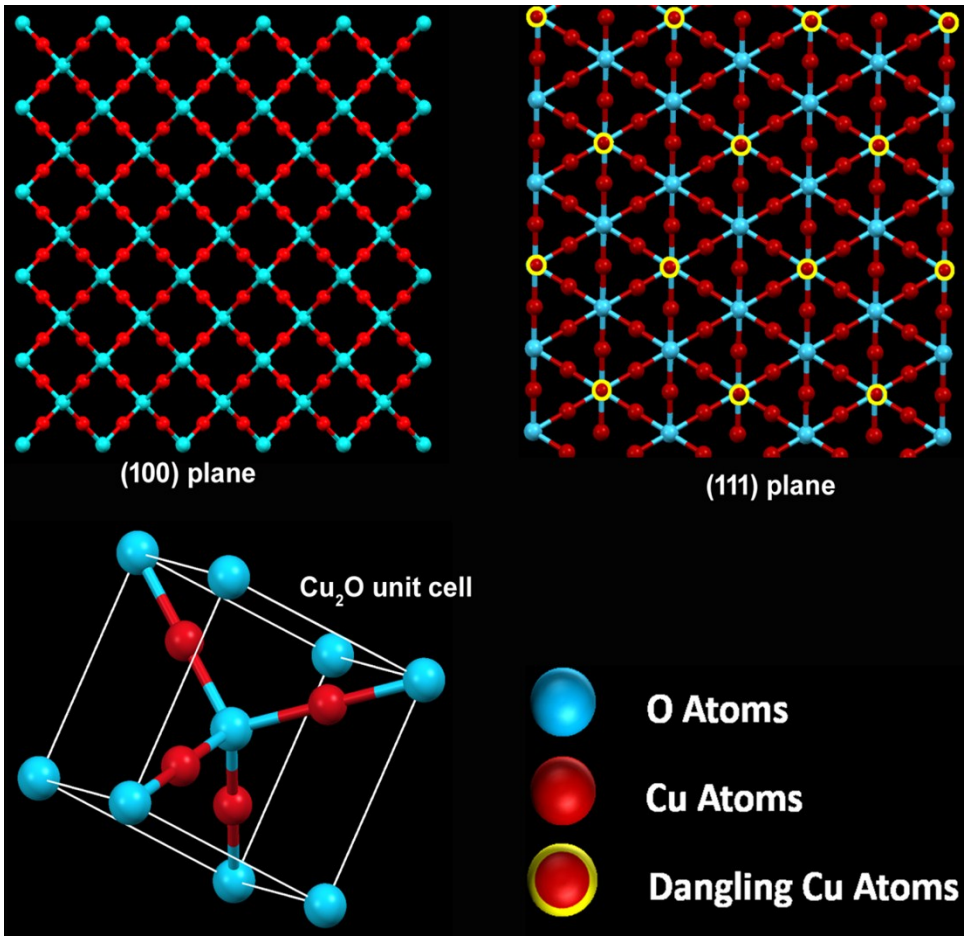

Figure S1: Crystal structure of Cu_2O with (100), (111) planes, and unit cell structure. The Cu atoms with dangling bonds are highlighted with yellow circles (All representations were obtained using Mercury 3.8 Software).

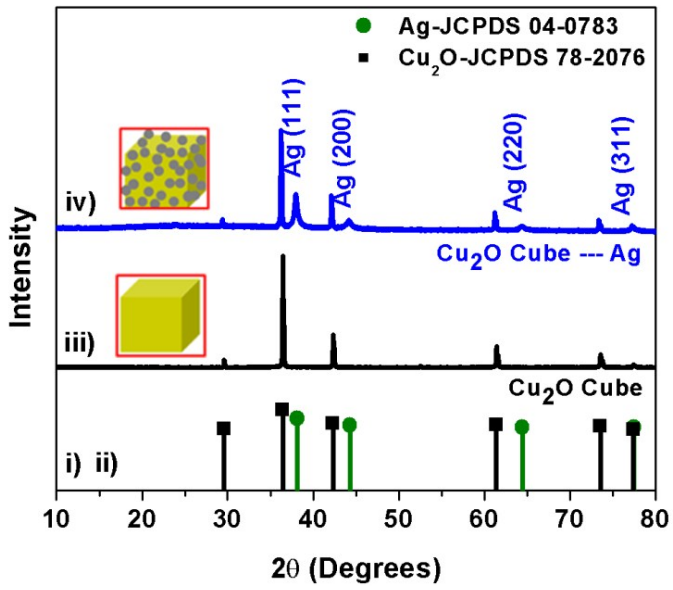

Figure S2: Powder XRD pattern of i) standard Cu_2O JCPDS file 78-2076, ii) standard Ag JCPDS file 04-0783, iii) Cubic Cu_2O particles, and iv) Cubic Cu_2O-Ag composite hetrostructure.

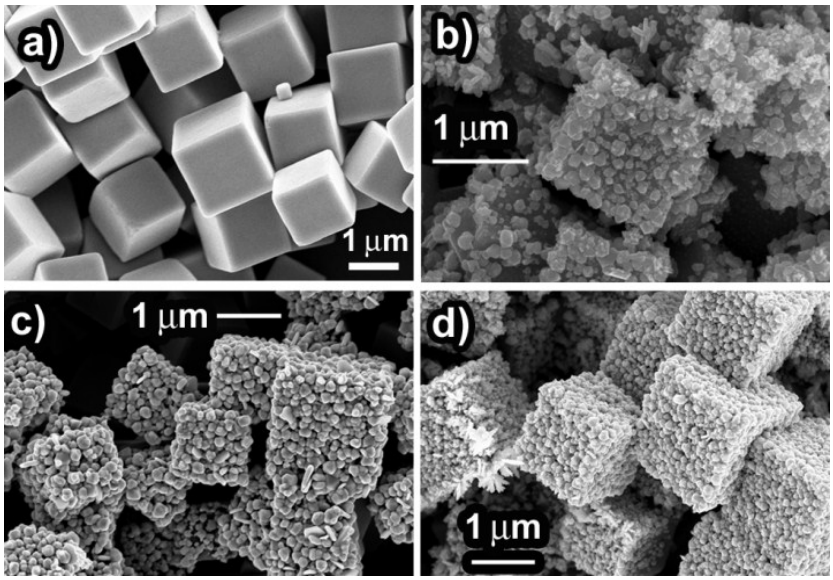

Figure S3: a) FESEM image of Cu_2O cube before GRR. b-d) FESEM image of cubic Cu_2O-Ag heterostructures after undergoing GRR with increasing [$AgNO_3$] solution clearly showing increased loading density of Ag NPs decorating the cubic Cu_2O surface.

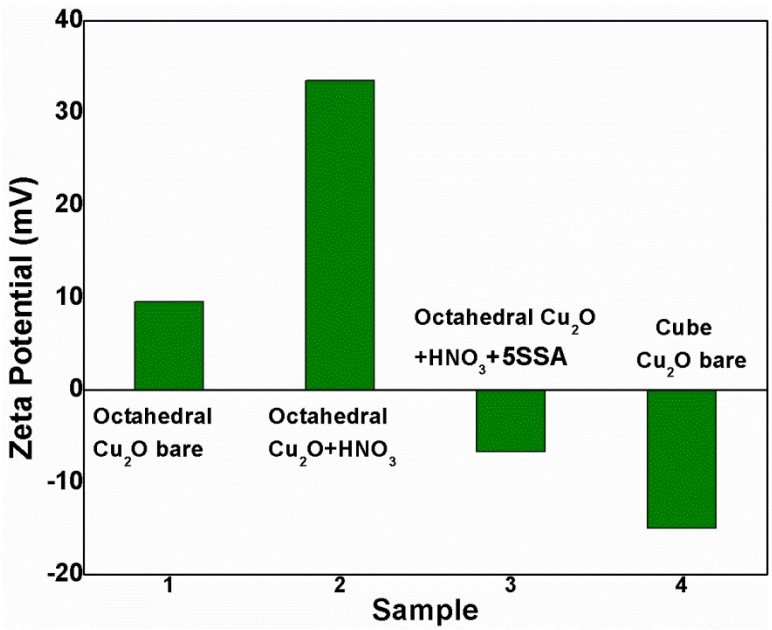

Figure S4: Zeta potential values measured for different samples under the experimental conditions.

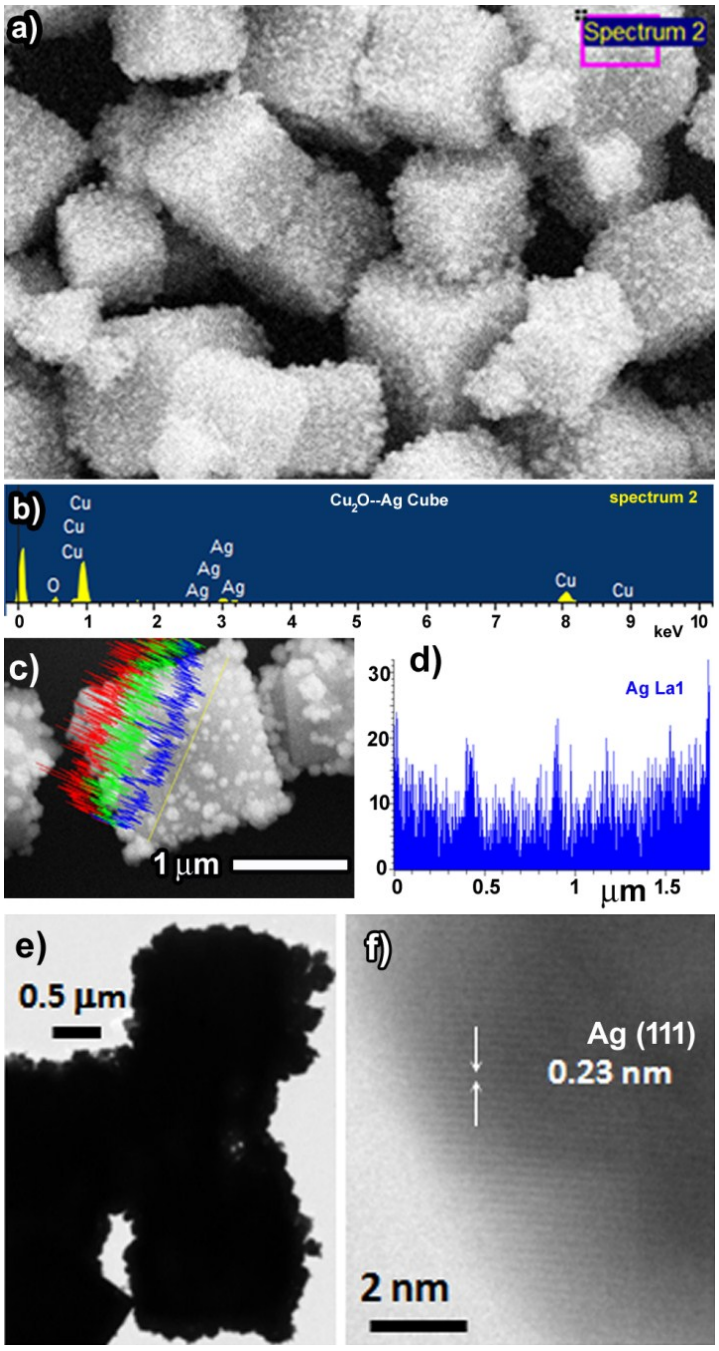

Figure S5: EDS spectrum of the (b) Cubic Cu_2O-Ag heterostructures from the highlighted region of the sample shown in (a) Line-scan EDS analysis of a (c-d) cubic Cu_2O-Ag heterostructure clearly identifying the Ag NPs decorating the surface of Cu_2O particles. TEM image of e) cubic Cu_2O-Ag heterostructure; f) observed lattice fringes from Ag NPs on the cubic Cu_2O-Ag heterostructure.

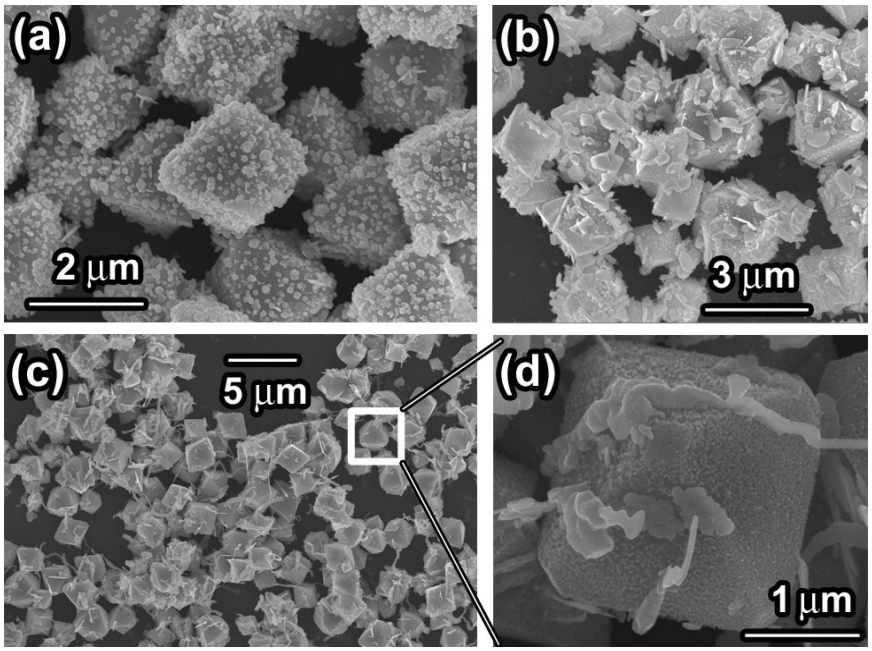

Figure S6: Effect of nitric acid and 5SSA on the morphology of the heterostructure: a) Cu_2O octahedra undergoing GRR with silver nitrate in presence of a) nitric acid and 5SSA; b) nitric acid only c) 5SSA only; d) magnified view of c).

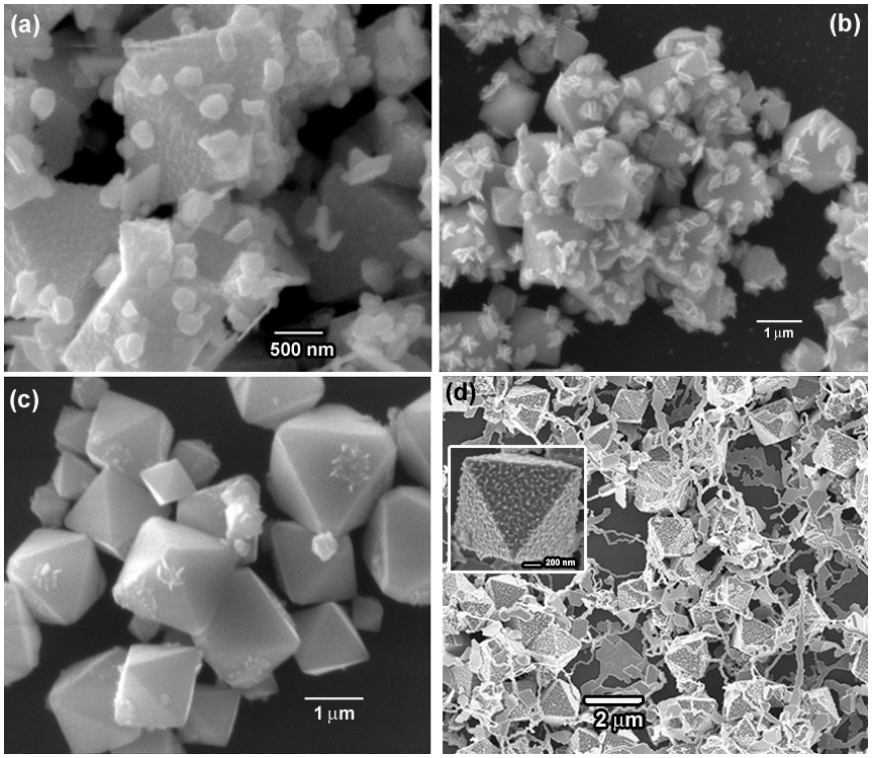

Figure S7: Effect of different surfactants on the morphology of the attained Cu_2O-Ag heterostructures : a) Oxalic acid, b) Citrate, c) SDS, d) PVP

Table S1: Peak frequencies (cm^{-1}) and their assignments for SERS/Raman spectra of p-MA.

Reference Raman	SERS	Peak Assignment
1598		νCC (a_1)
1572	1576	νCC (b_2)
1490	1475	νCC + δCH (a_1)
1480		νCC + δCH (a_1)
1445	1436	νCC + δCH (b_2)
1403	1390	δCH + νCC (b_2)
1310	1308	νCC + δCH (b_2)
1266		νCH(a_1)
1206		νCH(a_1)
1173	1191	δCH(a_1)
1142	1144	δCH (b_2)
1118		δCH (b_2)
1089	1078	νCS + νCC(a_1)
1011	1007	γCC + γCCC (a_1)
960	950	πCH(a2)
	921	πCH (b_1)
820	820	πCH (b_1)
	750	πCH (b_2)
	723	πCH + πCS + πCC (b_1)
633	634	γCCC (a_1)

ν-stretch; δ,γ-bend; π-wag; a_1, b_2: in plane mode; a_2, b_1: out of plane mode of benzene ring vibrations

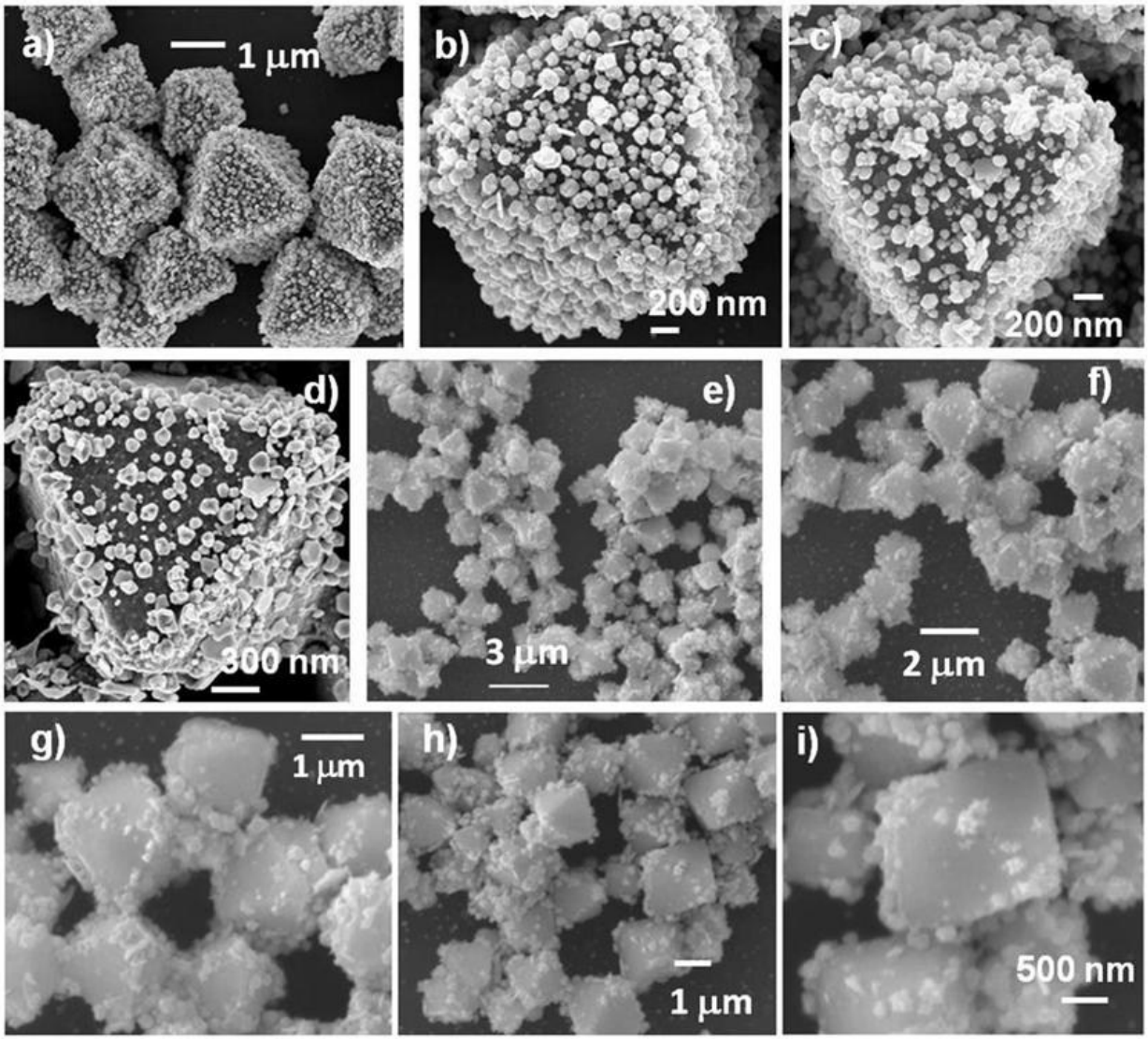

Figure S8: SEM images showing selective deposition of tips and edges, followed by facets for Cu_2O octahedral for 5SSA-Ag+ system at increasing concentration. At low concentrations, tips and edges get preferentially decorated (e-i) with no deposition on the facets. At increased concentration, facets start progressively decorating ultimately leading to fully decorated octahedral (a-d) heterostructures. Utilized [$AgNO_3$] are: h-i) 10mM; e-g) 20mM; d) 50mM; b-c) 75mM; a) 100mM respectively.

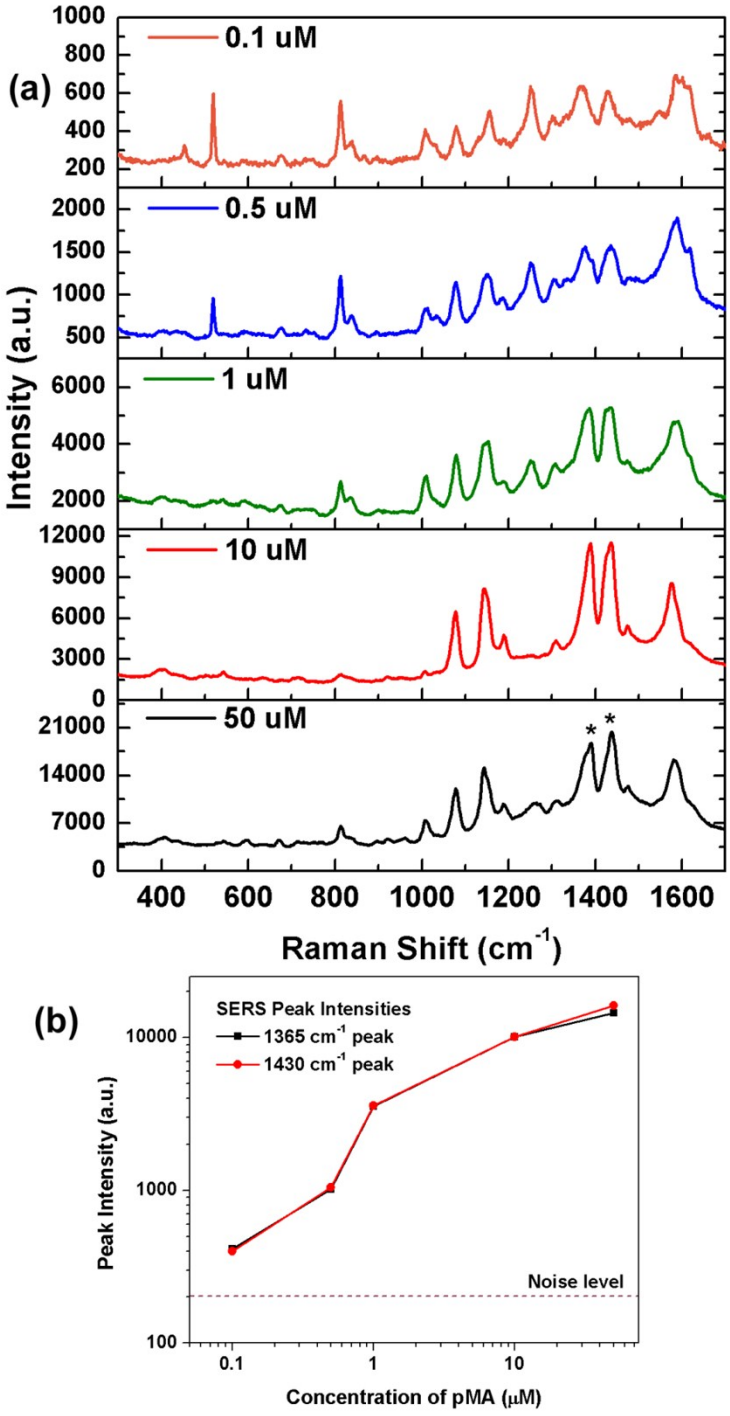

Figure S9: a) SERS spectra of p-MA at different concentrations showing the change in the SERS signal, b) Intensity of highlighted peaks (1365, 1430 cm^{-1}) as a function of p-MA concentrations.

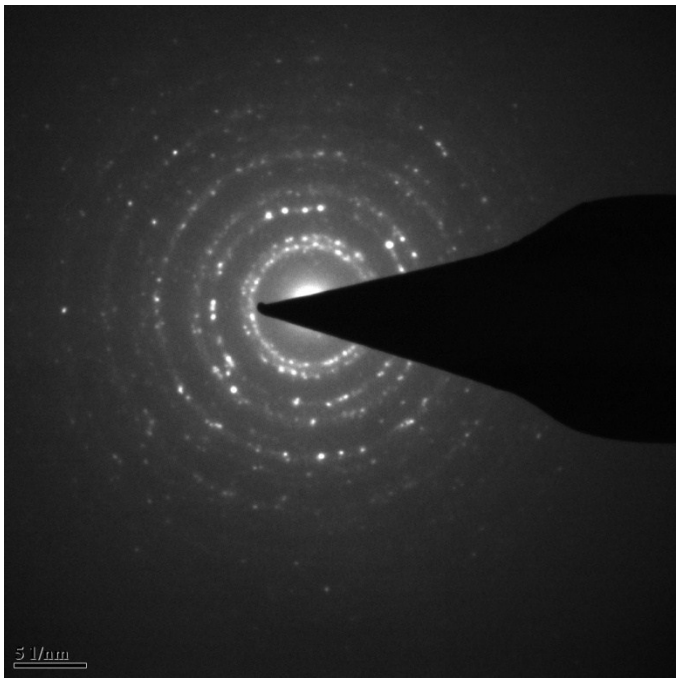

Figure S10: SAED pattern collected from a Au-Ag hollow mesocage showing the polycrystalline nature of the Au and Ag NPs comprising the mesocage.

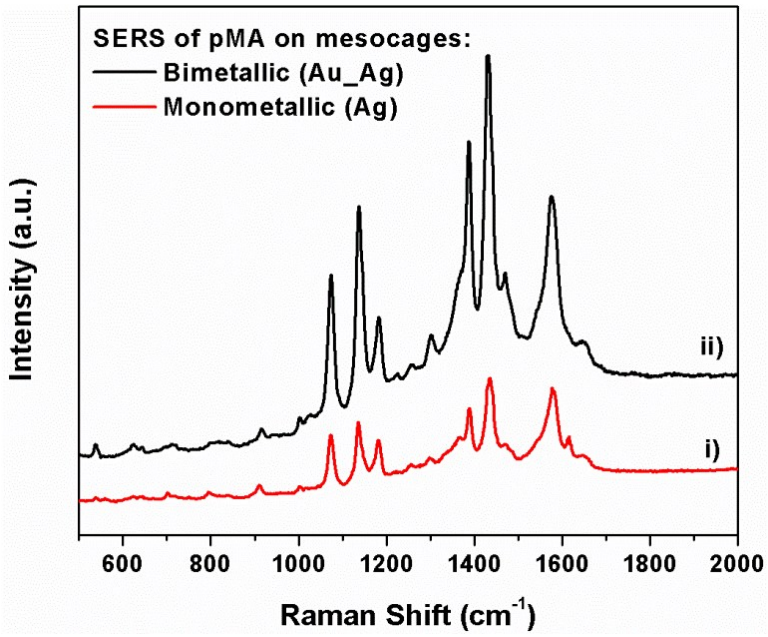

Figure S11: SERS spectra of pMA acquired using i) monometallic Ag and ii) bimetallic Ag-Au hollow mesocages as SERS substrate.

Table S2: Elemental concentrations as obtained using ICP-AES analysis

Au-Ag-Cu2O heterostructure		
Cu(ppm)	Ag(PPM)	Au(ppm)
4119.04	114.62	8.69
Au-Ag hollow mesocages		
Cu(ppm)	Ag(ppm)	Au(ppm)
4.5	85.3	8.65